Journal Pre-proof

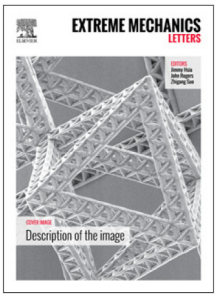

Strength of magnesium at high pressures and strain rates

Suraj Ravindran, Zev Lovinger, Vatsa Gandhi, Michael Mello, Guruswami Ravichandran

PII: S2352-4316(20)30248-0
DOI: https://doi.org/10.1016/j.eml.2020.101044
Reference: EML 101044

To appear in: *Extreme Mechanics Letters*

Received date : 15 May 2020
Revised date : 2 August 2020
Accepted date : 26 September 2020

Please cite this article as: S. Ravindran, Z. Lovinger, V. Gandhi et al., Strength of magnesium at high pressures and strain rates, *Extreme Mechanics Letters* (2020), doi: https://doi.org/10.1016/j.eml.2020.101044.

STRENGTH OF MAGNESIUM AT HIGH PRESSURES AND STRAIN RATES

Suraj Ravindran [1], Zev Lovinger [1], Vatsa Gandhi[1], Michael Mello[2], Guruswami Ravichandran [1,2]

[1]*Graduate Aerospace Laboratories, California Institute of Technology, Pasadena, 91125*

[2]*Department of Mechanical Engineering, California Institute of Technology, Pasadena, 91125*

Corresponding author: surajrav@caltech.edu (S. Ravindran)

Abstract

The strength and deformation mechanisms in magnesium can be significantly affected by anisotropy, high strain rates, and pressure. In this study, pressure shear plate impact (PSPI) experiments are conducted to measure the strength of extruded polycrystalline magnesium at pressures varying from 5-10 GPa at a nominal strain rate of 10^5 s^{-1}. The experimental technique enables to first shock load the material sample to the desired normal stress in one direction, and then shear the material in a perpendicular direction. A recently developed hybrid analysis method for PSPI experiments is used to extract the stress-strain curves of magnesium from the particle velocity records measured at the rear surface of the target. The PSPI experimental results reveal a slower twinning saturation at high pressures. To better understand the material behavior under the combined stress states in the PSPI experiments, the results were compared with that of a specimen deformed by a two-step process of quasi-static compression followed by dynamic shear loading at relatively low pressure. The two-stage loading at low pressure, and the calculation of temperature rise in the PSPI experiment revealed that the combined effect of the reorientation and the temperature rise lower the flow strength of magnesium at high pressures under multiaxial loading.

1. Introduction

Metals and their alloys with high specific strength are extremely desirable for advanced aerospace, automotive, and defense applications. Magnesium alloys are lightweight structural materials with a specific strength that is higher than the commonly used lightweight materials such as aluminum and titanium alloys. Also, there has been considerable interest in developing lightweight magnesium alloys with better performance for the aforementioned applications. In applications involving blast and impact, the materials are subjected to extreme loading conditions, which generate high pressures and strain rates. Therefore, understanding the deformation behavior of these materials under such loading conditions is vital to developing alloys with superior performance.

Magnesium has strong plastic anisotropy due to its hexagonal close-packed structure (HCP). There have been several experimental studies at strain rates ranging from 10^{-4}-10^{4} s^{-1} to understand the deformation behavior of magnesium and its alloys [1–6]. It has been shown that plastic deformation in magnesium is accommodated through basal slip, non-basal slip, and twinning. Basal slip and extension twinning are found to occur during deformation since they have the lowest critical resolved shear stress (CRSS), ~0.5 and 5 MPa, respectively [7,8]. These mechanisms are dominant in low rate experiments and appear to be rate-independent. In contrast, high CRSS (~ 45 MPa) prismatic slip is rate-dependent and plays a significant role in the strain rate-dependent behavior of magnesium. These high rate studies are limited to the rate-dependence on the strength of magnesium, whereas in high speed impact loading conditions, the pressure may also have a strong influence on the strength. However, there have been only limited studies towards understanding the effect of pressure on the strength of materials.

Recently, Turneaure et al. [9] performed shock and release experiments on magnesium single crystals and showed that the twinning is not active during the c-axis compression. Renganathan et al. [10] showed through a combination of experiments and numerical simulations that twinning forms in single-crystal magnesium when compressed along the a-axis. However, the strength behavior of magnesium at these pressures requires further exploration for developing robust material models in these loading regimes.

The main experimental measurement techniques available to measure the strength of materials at high pressures are based on lateral stress measurement using stress gages, shock release experiments, and pressure shear plate impact experiments (PSPI). PSPI experiments are advantageous over the other techniques because a complete stress-strain curve can be constructed from these experiments with high fidelity [11–15]. Millet et al. [16] conducted impact experiments to measure strength in AZ61 magnesium alloy using the lateral gage measurement technique and showed that the flow strength increases from 230 MPa to 1.2 GPa when pressure increases from 1 GPa to 7 GPa. Recent PSPI experiments conducted on AZ31B magnesium alloy explored the multiaxial stress behavior and showed a shear strength close to 180 MPa at 3.8 GPa pressure [17]. The results of this investigation deduced from the postmortem studies showed that significant extension twinning and reorientation of the crystals occur in the material during loading. Under extreme loading conditions, magnesium has very complex deformation mechanisms and

understanding them require further investigation in the higher-pressure regime. In this study, experiments are conducted using the PSPI technique at pressures ranging from 5 to 10 GPa to understand the effect of multiaxial loading and pressure on the strength behavior.

2. Materials and methods

Pressure shear plate experiments were conducted using a powder gun with a keyed barrel, which is 38.7-mm in bore diameter and 3-m in length. Detailed information on the experimental facility can be found in [18]. In this study, we adopt two different PSPI configurations involving symmetric plate impact of sandwiched (Fig. 1a) and symmetric anvil plate configurations (Fig. 1b) to investigate the strength of pure magnesium.

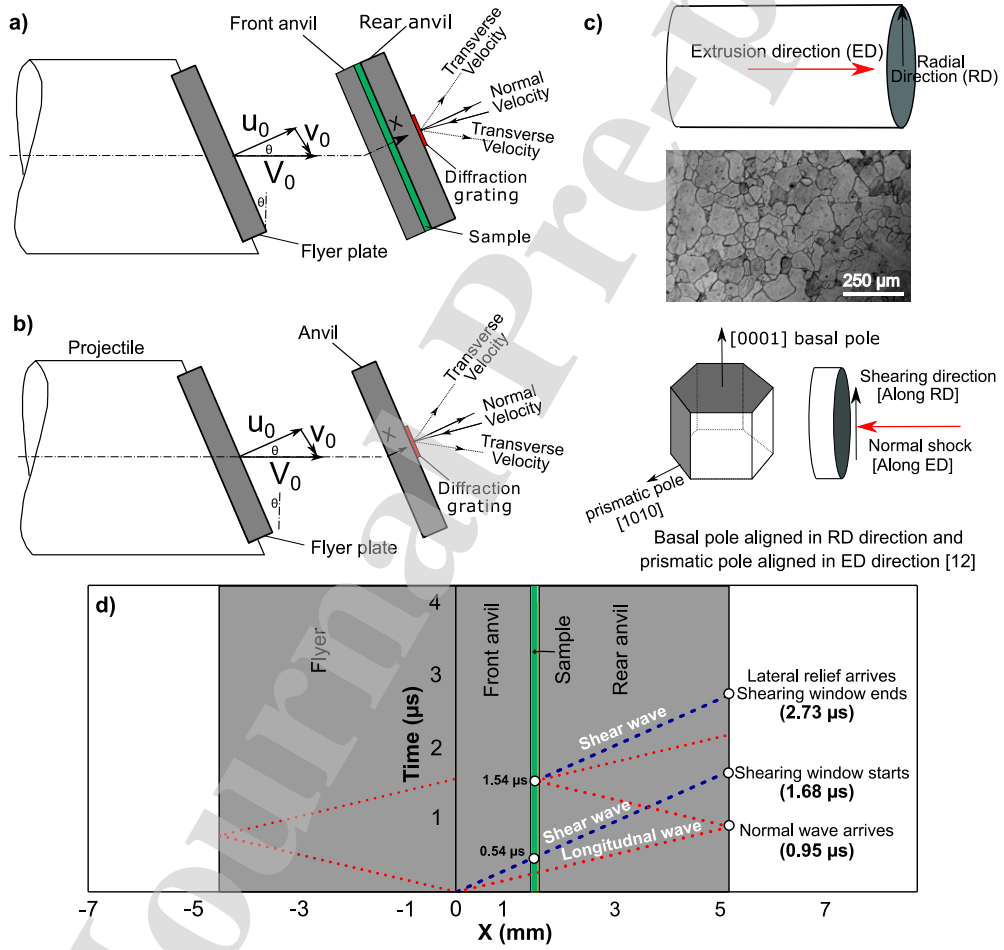

Figure 1. a) PSPI sandwich configuration, b) PSPI symmetric impact configuration, c) microstructure, crystal orientation, and the loading directions for magnesium, d) distance-time (X-t) diagram of the sandwich configuration PSPI experiment.

In PSPI experiments, the flyer is skewed with the horizontal axis of the gun barrel to generate both normal and shear waves upon impact. In the sandwiched plate configuration, a thin magnesium sample is placed between the front and rear anvil plates (Fig.1a). The impedance of the anvil plates is usually higher than that of the sample in a sandwich configuration. During the sample preparation phase, the anvil plates and samples are lapped flat to within 1.65 μm, as indicated by three or less circular Fizeau interference fringes using a 550-monochromatic light source. The flyer and target assemblies are initially aligned using an autocollimator and flat mirror assembly to initially set the tilt angle below impact faces at well-below 1-milliradian (0.057^{o}).

The distance-time (X-t) diagram of the experiment shown in Fig.1d illustrates the wave loading history of the sample. The impact occurring at t=0 μs, generates both normal and shear waves in the front anvil plate, as shown in Fig.1d. Since the shear wave is slower than the longitudinal (normal) wave, the sample is initially swept by the normal wave and compressed. The normal wave reverberates within the lower impedance sample, and the normal stress equilibrates to the desired value before the arrival of the shear wave. The dimensions of the target assembly are chosen using the X-t diagram. Wave arrival calculations are based on the elastic wave speeds in the anvil plates (shown in Table 1). The normal wave traverses through the sample and arrives at the free surface of the rear anvil plate at approximately 0.95 μs. The normal wave is reflected back towards the sample as an unloading wave. The shear wave arrives in the sample at approximately 0.54 μs and continues to shear the sample at constant pressure until the normal unloading wave arrives from the rear surface at 1.54 μs. The 1 μs interval between the arrival of the shear and unloading waves is herein referred to as the shear-window. During this interval, the sample undergoes significant shearing deformation, and this information propagates to the free surface of the rear anvil plate, where PDV and HTV interferometers record the normal and transverse particle velocity profiles [19]. In addition to the normal and shear waves, lateral release waves are generated from the circular boundaries of the front anvil plates upon impact. The release waves propagate diagonally toward the center of the sample at the longitudinal wave speed and ultimately limit the duration of the measurement. In the current experimental design, the arrival of the lateral release wave at 2.73 μs after the impact ensures a state of simple shear at constant pressure for the duration of the shear-window. The strength of the sample at the designed pressures is inferred from the particle velocity profiles recorded during this time. Particle velocity data recorded after the arrival of the lateral release wave is not used in the strength calculation.

Conventionally, the sandwiched-anvil PSPI experiments are conducted using elastic anvils at relatively low pressures [20]. This approach enables a straightforward calculation of the shear stress-strain curve of the sample using the elastic impedance of the anvils. However, at pressures exceeding the Hugoniot elastic limit (HEL) of these anvil materials, elastic analysis is no longer valid. Therefore, a recently developed simulation-based methodology is required to construct the stress-strain behavior of the material [21]. In this method, a material model is first calibrated for the anvil plates at similar pressures and strain rates using the symmetric PSPI configuration shown in Fig. 1b and numerical simulation. The present study uses D2 tool steel (McMaster Carr, Los Angeles, CA) as the anvil material. Two symmetric PSPI experiments were conducted on anvil plates to calibrate a material model for the D2 tool steel. The skew angle (θ) of 18° was chosen for all the experiments. The dimensions of the anvil plates and the samples are shown in Table 2.

As-received extruded polycrystalline magnesium samples of 99.99% purity obtained from the Goodfellow Corporation were used in this study. The microstructure of the sample is shown in Fig. 1c and the average grain size was measured to be 68 μm. For the pressure shear experiments, samples of 30 mm diameter and 2 mm thickness are first extracted from a 50 mm diameter cylinder. These samples are lapped down to 300±1 μm thickness. This specific thickness was chosen to ensure that there are at least three crystals along the thickness direction to be roughly the representative volume of the material. It is well-known that the extruded sample has a strong texture with the c-axis aligned in the radial direction, as shown in Fig. 1c [1,22]. In the PSPI experiments, the normal loading was applied along the extrusion direction (ED), which corresponds to a-axis compression of single-crystal magnesium. The shearing was applied along the radial direction (RD), as depicted in Fig. 1c. Table 1 shows the density and elastic wave speeds of the materials used in the present work.

Table 1. Density and wave speeds in the anvil plates and sample

Material	Longitudinal wave speed (m/s)	Shear wave speed (m/s)	Density (kg/m^3)
D2-tool steel	5,860	3,120	7,900
Magnesium	5,840	3,050	1,740

3. Results and Discussion

The impact conditions, physical dimensions of the anvils, and samples for all the experiments conducted in this study are shown in Table 2. The first set of experiments were conducted to characterize the D2 tool anvils using the symmetric PSPI loading configuration (Fig. 1b). The second set of experiments using the sandwich configuration (Fig. 1a) was conducted on magnesium to measure the strength of these samples.

Table 2. Summary of the experiments and the dimensions of the flyer, anvil, and sample

Experiment	Impact velocity (V_0) (m/s)	Skew angle (θ) (degree)	Flyer Plate* (mm)	Front anvil* (mm)	Rear anvil** (mm)	Anvil	Magnesium sample thickness** (mm)	Tilt (mrad)
Symmetric	539	18	5.47	3.98	-	D2 steel	-	0.42
Symmetric	645	18	6.49	3.96	-	D2 steel	-	0.35
Sandwich	298	18	5.78	1.54	3.7	D2 steel	0.297	0.61
Sandwich	545	18	5.74	1.58	3.7	D2 steel	0.300	0.60

*diameter of the flyer and front anvil plates is 34 mm for symmetric PSPI and sandwich PSPI experiments. **diameter of the rear anvil plate and the sample is 30 mm.

3.1. Anvil tool steel material model calibration

The free surface normal and transverse particle velocity profiles for the two symmetric plate impact experiments conducted at 539 m/s and 645 m/s are shown in Fig. 2a. The experimental velocity profiles are shifted in time for clear visualization. Corresponding normal and transverse particle velocity components for the PSPI experiment conducted at impact velocity 539 m/s (V_0) are 512 m/s ($V_0\cos\theta$) and 166.5 m/s ($V_0\sin\theta$), respectively. For the second experiment conducted at impact velocity 645 m/s (V_0), the normal and transverse velocities are 613 m/s ($V_0\cos\theta$) and 199 m/s ($V_0\sin\theta$), respectively. In both experiments, the measured free surface normal velocity profiles closely approach the value of the normal velocity component, as expected, in the case of symmetric impact experiments. The normal stress in the sample is close to 10 GPa for the experiment conducted at 539 m/s (V_0) and 12 GPa for the second experiment conducted at 645 m/s (V_0). The normal free surface particle velocity profile shows the typical shock behavior of elastic-plastic materials [23]. The normal velocity corresponding to the HEL of the D2 tool steel is close to 70

m/s. In both the experiments, the HEL (~ 1.6 GPa) is close to 70 m/s, indicating the robustness and reliability of the measurements. The transverse profile shows relatively linear behavior in time, as seen in Fig. 2a. This feature is mainly due to the dissipation of the shear wave as it travels through the plastically deforming target plate [18].

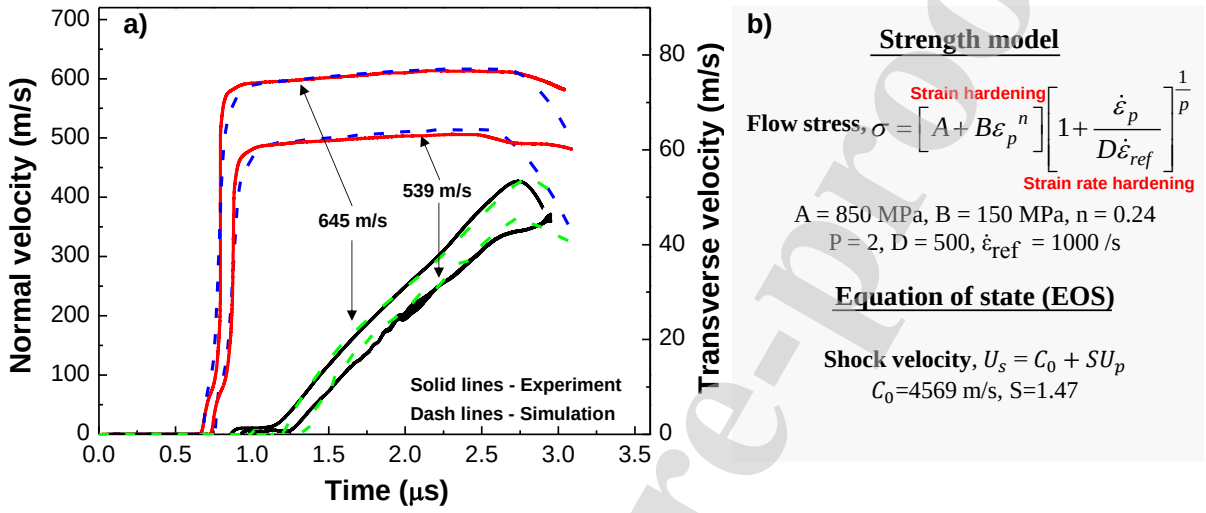

Figure 2. Symmetric experiments on D2 steel at 539 m/s and 645 m/s: a) comparison of normal and transverse free surface velocities - experimental vs. simulations, b) D2 strength model and equation of state (EoS) in the numerical simulations with the corresponding calibrated parameters.

The numerical simulations in this study are performed using the finite element software, Abaqus [24], modeling the 3-dimensional geometry of the sample assemblies. The interface between the flyer and front plate is modeled using a contact surface with a high friction value. This allows for the actual impact to occur (accounting also for experimentally measured tilt values between the flyer and target) without the possibility of slip when the plates come in contact. The nodes on the sample interfaces are tied to the nodes on the front and rear anvil plates. In order to capture the shock rise time, an element size of 25 μm was found to be optimal for achieving converged results.

The strength of the material is calibrated using a power-law strain hardening and the Cowper-Symonds strain rate hardening models, as shown for the flow stress equation in Fig. 2b. The volumetric behavior of the material is modeled using a linear Grüneisen equation of state (EOS) [25]. The parameters for the strength model are systematically varied until the best match to both

the normal and transverse velocity profiles from the experiments is obtained. The final matched profiles, along with the calibrated parameters obtained from the simulation are shown in Fig. 2.

3.2. Free surface particle velocity profiles for magnesium sandwich experiments

Measured free surface normal and transverse velocities corresponding to impact speeds of 298 m/s and 545 m/s from experiments conducted on magnesium using the sandwiched anvil configuration (Fig. 1a) are shown in Fig. 3. The corresponding pressures for the two experiments are 5.6 GPa and 10.5 GPa, respectively. Interestingly, the shearing rates for both the experiments are close to 1.5×10^5 s^{-1} despite the difference in the imposed transverse velocities. The normal velocity profile shows very similar behavior, as observed in the symmetric steel experiments (Fig. 2a). During the normal shock, the steel anvils undergo plastic deformation (1.5 % at 5 GPa and 3.5 % at 10 GPa), and hence, the normal behavior of the thin sample does not substantially affect the normal velocity profile. However, the transverse velocity profile is distinctly different from that observed in the symmetric steel experiments and reflects the strength of the magnesium sample sandwiched between the anvil plates. It is noted, in both experiments, the transverse velocity profile is initially negative. The reason for this behavior is addressed later. In the lower impact velocity experiment (298 m/s), the transverse velocity profile shows the sigmoidal characteristic, whereas, at higher impact velocity (545 m/s), relatively linear response is observed.

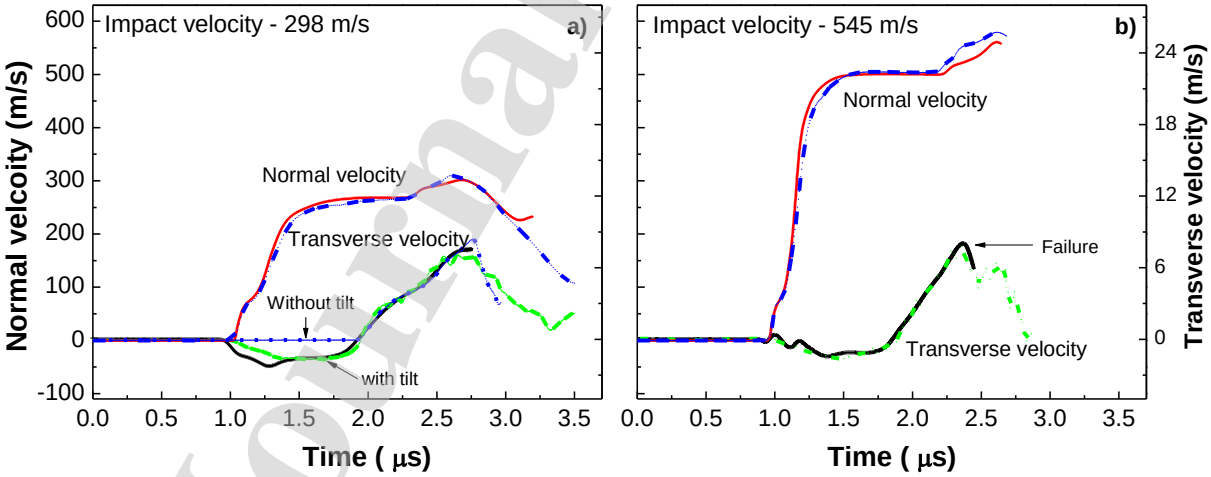

Figure 3. Normal and transverse velocity profiles for the pressure shear plate impact experiments on magnesium at impact velocities of 298 m/s and 545 m/s along with corresponding results from converged simulations. The solid lines are the experimental results and the dashed lines are results from simulations.

The volumetric behavior of magnesium is modeled using a linear Grüneisen equation of state (EOS). Parameters for the Us-Up relation is obtained from [25]. The strength model for magnesium used in the simulations includes the Cowper-Symonds strain rate hardening function and an isotropic strain hardening function, as shown in Eq. (1). The strain hardening function for magnesium includes besides the linear term, an additional exponential term to account for the sigmoidal behavior observed in the experiments. The linear hardening term is used to capture the flow behavior after initial yielding, which is controlled by twinning and prismatic slip. After the twinning is exhausted, the stress-strain curve transitions to a steeper behavior, which is possibly controlled by pyramidal slip due to hard orientations which result from the reorientation of the crystals as a result of twinning. This behavior is strongly dependent on pressure, as explained earlier. The strain hardening behavior (expressed with parameters B and C) is changed to adjust the pressure dependence of the complex strain hardening evolution between the two pressures, which is not included explicitly in the model. For the final parameters shown in Table 3, the normal and transverse velocity profiles from the simulations matched quite well with the experimentally measured profiles. It is noted, a single set of parameters could not predict the behavior because the pressure dependence of yield strength is not included. Therefore, the parameters of the model had to be changed accordingly to match the velocity profile observed in the study. For the higher impact velocity experiment, a strain-based failure criteria (no strength at a critical strain) with the critical strain set at 0.15 was needed to match the measured drop in the transverse velocity.

$$\sigma = \left[A + B\varepsilon_p + C\exp\left[\left(\frac{\varepsilon_p}{a}\right) - 1\right]\right]\left[1 + \frac{\dot{\varepsilon}_p}{D\dot{\varepsilon}_{ref}}\right]^{\frac{1}{p}} \quad (1)$$

Table:3 Fitted model parameters (Eq. (1)) for magnesium

Experiment	A (MPa)	B (MPa)	C (Pa)	a	D	$\dot{\varepsilon}_{ref}$ (1/s)	p
5.6 GPa	42 .1	500	900	0.01	500	1000	2
10.5 GPa	42.1	1400	60	0.01	500	1000	2

To understand the linear transverse velocity profile in the 10.5 GPa experiment, the normal strain (1- ρ_0/ρ, ρ_0=initial density, ρ=density after compression) induced by the normal shock is calculated from the Hugoniot data available for magnesium [25]. It is noted that at 5.6 GPa, the normal strain

is ~0.11 before the shear wave arrives, whereas, at 10.6 GPa, the shock generates a normal strain ~0.16 due to the high compressibility of magnesium. This observation indicates that at 10.5 GPa, the normal shock could exhaust most of the twinning before the shear wave arrives. To estimate the volume fraction of twinning during normal compression before the shear wave arrives, the approach developed by Johnson et al. [26] is used. The volume fraction of twinning is given by,

$$V_{ftwin} = \left[\frac{1}{T_R} \int_0^t \left(\frac{\tau}{\tau_0} - 1 \right) dt \right]^m \; if \; \tau > \tau_0 \tag{2}$$

where, the model parameters T_R =2 μs, τ_0 = 6 MPa, m=3 are obtained from Renganathan et al. [10]. The resolved shear stress (τ) was calculated from the normal and lateral stresses in the sample, obtained from the numerical simulation. The volume fraction of twinning was calculated to be 43% at 5.6 GPa. The critical pressure at which the twinning saturation occurs was calculated to be 7.5 GPa, lower than the 10.5 GPa of the higher velocity impact experiment. However, it is interesting to note that these equations do not account for the pressure dependence of the twinning formation. Xu et al., have shown that the nucleation stress for twinning increases with pressure [27]. Therefore, the twinning saturation calculated with this analytical formulation [26] may not be accurate and needs to be used with caution in the high-pressure regime.

To investigate the initial negative dip in the transverse velocity in both the experiments, the flyer is tilted with respect to the front anvil in the 3D numerical simulation of the experiment. The tilt and the relative orientation between impacted plates in the simulations correspond to the tilt angle and orientation between the flyer and target plates obtained from the experiments. It is observed in Fig. 3, the 3D numerical simulation with tilt captures the dip in the transverse velocity. The tilt does not affect the peak transverse velocity; therefore, the effect of tilt can be neglected in the strength calculations.

3.3. Equivalent stress-strain curve and temperature rise

The equivalent stress-strain curve (Fig. 4a) was constructed by matching the normal and transverse velocity profiles from the PSPI experiments. The stress-strain curve obtained using the split Hopkinson (Kolsky) pressure bar (SHPB) technique is also shown to compare with the stress-

strain behavior of the material at nominally without any pressure (<0.1 GPa). Note that the compression was performed along the ED direction, and the strain rate in the SHPB experiment was ~2.0×10^3 s^{-1}, two orders of magnitude lower than the strain rate in the PSPI experiments.

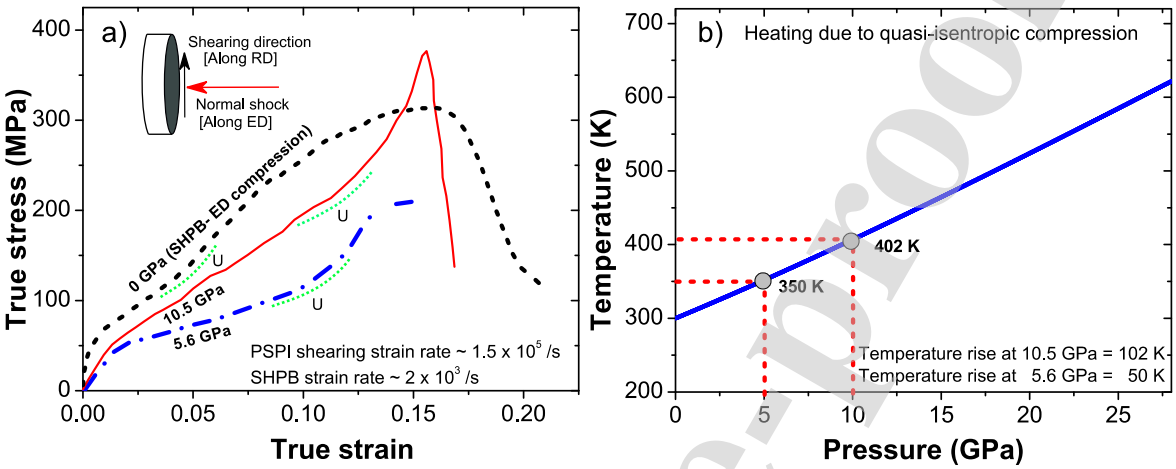

Figure 4. a) True stress-strain curve at 10.5 GPa, 5.6 GPa, and <0.1 GPa (SHPB) experiments, b) calculated temperature in the sample due to the quasi-isentropic compression of the sample.

Equivalent stress-strain behavior at pressures of 5.6 GPa and 10.5 GPa shows the characteristic sigmoidal stress-strain behavior observed in magnesium when the compression loading is performed along the ED of the material [1]. This sigmoidal shape is associated with the profuse extension twinning in the sample. Renganathan et al. [10] showed that deformation in pure single crystal magnesium is accommodated through prismatic slip and extension twinning when shocked along the a-axis. In the present study, the compression occurs along the ED direction, which is close to the a-axis compression since the c-axis is aligned along the RD in extruded magnesium. Two characteristics of the stress-strain curves are noteworthy. 1) a steeper strain hardening response at 10.5 GPa compared to the 5.6 GPa experiment, and 2) the upturn (marked as U) in the stress-strain curve seems to be delayed at high pressures. The initial hardening region, in the beginning, is mainly attributed to the extension twinning, basal slip, and prismatic slip in the material. After the upturn, the stress-strain curve mostly corresponds to slip dominated deformation of the material. The upturn in the stress-strain curve corresponds to the saturation of extension twinning and indicates that at higher pressures and strain rates the twinning saturation is delayed. It is further evident when comparing it with the stress-strain curve obtained from the compression along ED direction of a 4 mm cubic sample in SHPB experiment in which the

saturation occurs at an axial strain of around 0.06. Whereas, in the high pressure PSPI experiments, these upturns correspond to the equivalent strain of 0.08 and 0.12. Also, the strength at a given strain at 10.5 GPa is higher compared to the experiment at 5.6 GPa. For both the PSPI experiments, as described before, the shearing strain rate is nominally the same; therefore, the observed strengthening behavior is solely a function of pressure (pressure hardening).

It is important to note that the strength observed in the low-pressure SHPB experiments is higher than that in the high-pressure experiments. Zhao et al. [18] also noted similar behavior in the experiments performed using pressure shear plate experiments on AZ31B magnesium alloy and attributed it to the anisotropic behavior of the material. There can be two possible causes for such behavior. The first is the temperature softening resulting from the temperature rise associated with the normal shock and shear deformation of the sample. The second is the reorientation of the crystals as a result of twinning due to the normal shock that occurs prior to the shearing of the sample.

Real-time temperature measurement in PSPI experiments would be ideal for estimating the thermal softening but technically challenging due to the short time scales (~μs) of the experiments. However, the temperature rise can be estimated based on the analysis developed in [14]. The temperature increase in the PSPI experiments has contributions from both the shear deformation and the normal shock. In the PSPI experiments, the final pressure is achieved after multiple reverberations within the sample, and the loading path is close to *quasi-isentropic* compression. Therefore, a conventional temperature rise calculation based on the entropy generation as a result of the shock jump is not required. In this study, the temperature rise due to the shear deformation is calculated based on Eq. (2) and the temperature rise due to normal shock is calculated based on Eq. (3) [14]. The temperature rises due to deformation for the two experiments at 5.6 and 10.5 GPa are estimated to be ~ 8 K and ~16 K, respectively. The estimated temperature rise in these experiments is close to the measured temperature in the dynamic compression of pure magnesium [4]. This rise in temperature is relatively small compared to the melting point (923 K) of the sample.

$$\text{Temperature rise due to deformation, } dT = \int \frac{\sigma d\varepsilon}{\beta C_p \rho_0} \tag{2}$$

$$\text{Temperature rise due to normal shock, } dT = \frac{\alpha T dp}{C_p \rho_0} \quad (3)$$

where β=0.9, assuming 90 % of the plastic work is converted to heat, pressure-dependent volumetric thermal expansion coefficient, $\alpha = a\exp(mP)$, a=7×10^{-5} K^{-1}, m=0.021 GPa^{-1}, T is temperature, P is pressure, and ρ_0 is the initial density of the material. Specific heat, C_p = (900+0.446T) J/kg [28].

A simple ordinary differential equation is solved using a 4th order Runge-Kutta method to calculate the temperature rise due to the initial period of loading where the sample undergoes only compression from the normal shock. The specific heat as a function temperature and the volumetric thermal expansion coefficient as a function of pressure is used, and the details are shown in Appendix 1. The temperature increase due to the normal compression is shown in Fig. 4b. The calculated temperature increase due to the initial compression for the experiments at 5.6 and 10.5 GPa was calculated to be 50 K and 106 K, respectively. It is important to note that the flow strength of magnesium is highly temperature dependent. It was seen that when the temperature increases from 298 K to 398 K, the peak flow stress of magnesium at a strain rate of 4000 /s decreases from 360 MPa to 275 MPa, a 20% reduction in strength [29]. Also, it was observed that the volume fraction of twinning reduces from 0.4 to 0.3 when the temperature increases from 298 K to 398 K [30], which is due to the reduction in CRSS of prismatic slip. Therefore, the delayed saturation observed at high pressures is possibly due to the temperature rise and the following transformation of the twinning dominated to the combined prismatic slip and twinning mechanisms.

3.4. Two-stage loading of the sample: Anisotropic response

A second possibility is the anisotropic response of the material as a result of the reorientation of the crystals when the normal shock propagates along the RD direction (favorable for twinning). Chen et al. [31] showed that when the shock compression applied along $\langle 10\bar{1}0\rangle$, the crystal reorients with the new c-axis at 86.3^0 with the old c-axis. This new c-axis was nearly parallel to the loading axis as shown in Fig. 5a. When the crystal is compressed along the $\langle 10\bar{2}0\rangle$, the c-axis reorients similarly, but the new c-axis is oriented at 30^0 with the loading direction. In the PSPI experiments, both of these mechanisms are active due to the strong texture of the material, which is favorable for such deformation during the normal compression. This reorientation enables low CRSS basal slip to be predominantly active along with prismatic slip.

Experiments are conducted in a similar loading pattern as in the PSPI experiment to investigate this possibility. First, the extruded samples are compressed along the ED to 16% of the normal strain using universal materials testing machine, see Fig. 5a. This loading saturates the twinning in the material, and the crystals reorient its c-axis along the ED. A modified hat specimen, named S-shaped samples developed by Arab et al. [32] is extracted from the cylinder. In the S-shaped specimen, the shearing direction is aligned along RD. The dimensions of the sample, shearing region, and the shearing area are shown in Fig. 5a. Complete details of the analysis to extract the stress-strain curve can be found in [32]. The samples are loaded using a conventional split Hopkinson pressure bar with *in situ* strain measurement using high-speed digital image correlation [33,34]. The conventional one-dimensional wave analysis is applied to calculate the shearing force [35]. The engineering shear stress in the sample is calculated using the measured shear force and the shearing area. The shearing strain is obtained from high-speed camera images using the digital image correlation (DIC) technique. The evolution of the shearing deformation is shown in Fig. 5b. The shearing rate for the experiments is ~4200 /s.

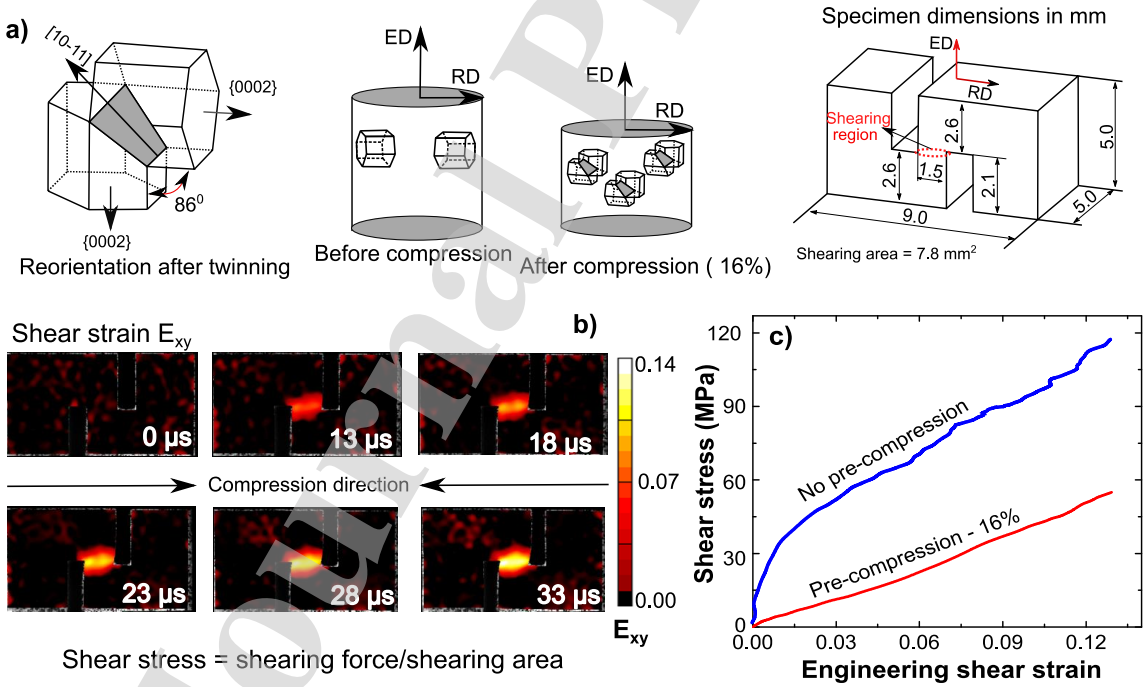

Figure 5. a) Reorientation of the crystal due to twinning, schematic of the pre-compression and reorientation, and dimensions of the S-shaped sample, b) local shear strain evolution in the gage

section during dynamic compression using SHPB, c) shear stress-shear strain curve for the pristine (no pre-compression) and pre-compressed (16%) samples.

Figure 5c shows the shear stress-shear strain curve obtained for the pre-compressed and pristine (no pre-compression) samples. The pre-compressed sample shows a distinct response with 50% reduction in strength compared to the pristine sample at an applied shear strain of ~0.12. It is clear that the reorientation of the crystal has a significant effect on the strength under multiaxial loading conditions. It is noted here, for the crystal that is reoriented along the shock direction will undergo predominantly basal slip and twinning with a small fraction of deformation accommodated by other deformation mechanisms such as prismatic slip. The crystal reoriented at around 30^0 with the loading axes will be favorable for combined prismatic slip and basal slip deformation mechanisms [36].

In the SHPB compression experiment on the cubic sample, the load is applied in the same direction for the entire duration, thus, after the saturation of the twinning, the hard orientations of the crystals cause the prismatic and the pyramidal slip to be activated. This causes relatively faster twinning saturation and the subsequent hardening. In contrast, in the PSPI experiments, after the normal shock passes, the shear wave loading has a new orientation which is favorable for the easier basal slip and possible twinning. In addition, the temperature increase due to the normal shock results in reduction of the CRSS for the prismatic slip which delays the twinning saturation. Due to both of these mechanisms, the strength appears to be lower under combined normal and shear loading. However, when comparing the strength between the two PSPI experiments where the samples undergo very similar reorientation and loading, the strength is seen to be strongly affected by the pressure.

4. Summary and conclusion

The mechanics and mechanisms of the deformation of pure magnesium at high pressures and strain rates is explored. In this study, pressure shear plate experiments are conducted to understand the effect of pressure on the strength of magnesium. A new simulation-based methodology is implemented to extract the stress-strain behavior of the magnesium at high pressures. When compared to the SHPB data at lower rates, the strength measured in PSPI experiment is smaller. A two-stage compression experiment revealed that the reorientation of the crystal due to the normal

shock causes low CRSS basal slip to be favorable during the shearing phase of the deformation. Also, the temperature increase appears to reduce the CRSS of the temperature dependent prismatic slip. Therefore, the combined effect from the temperature and reorientation lowers the strength of the material. However, when comparing the results between the PSPI experiments, the flow strength increases from 200 MPa to 300 MPa when the pressure increases from 5.6 to 10.5 GPa.

Acknowledgment

The research was sponsored by the Army Research Laboratory and was accomplished under Cooperative Agreement Number W911NF-12-2-0022. The views and conclusions contained in this document are those of the authors and should not be interpreted as representing the official policies, either expressed or implied, of the Army Research Laboratory or the U.S. Government. The U.S. Government is authorized to reproduce and distribute reprints for Government purposes notwithstanding any copyright notation herein. We also want to thank Dr.Christian Kettenbeil for making the diffraction gratings on the plates.

References

[1] N. Dixit, K.Y. Xie, K.J. Hemker, K. Ramesh, Microstructural evolution of pure magnesium under high strain rate loading, Acta Materialia. 87 (2015) 56–67.

[2] V. Kannan, X. Ma, N.M. Krywopusk, L.J. Kecskes, T.P. Weihs, K. Ramesh, The effect of strain rate on the mechanisms of plastic flow and failure of an ECAE AZ31B magnesium alloy, Journal of Materials Science. 54 (2019) 13394–13419.

[3] N. Dudamell, I. Ulacia, F. Gálvez, S. Yi, J. Bohlen, D. Letzig, I. Hurtado, M. Pérez-Prado, Twinning and grain subdivision during dynamic deformation of a Mg AZ31 sheet alloy at room temperature, Acta Materialia. 59 (2011) 6949–6962.

[4] D. Ghosh, O.T. Kingstedt, G. Ravichandran, Plastic work to heat conversion during high-strain rate deformation of Mg and Mg alloy, Metallurgical and Materials Transactions A. 48 (2017) 14–19.

[5] O.T. Kingstedt, J.T. Lloyd, On the conversion of plastic work to heat in Mg alloy AZ31B for dislocation slip and twinning deformation, Mechanics of Materials. 134 (2019) 176–184.

[6] V. Kannan, K. Hazeli, K. Ramesh, The mechanics of dynamic twinning in single crystal magnesium, Journal of the Mechanics and Physics of Solids. 120 (2018) 154–178.

[7] E. Kelley, W. Hosford, Plane-strain compression of magnesium and magnesium alloy crystals, Trans Met Soc AIME. 242 (1968) 5–13.

[8] H. Yoshinaga, R. Horiuchi, On the nonbasal slip in magnesium crystals, Transactions of the Japan Institute of Metals. 5 (1964) 14–21.

[9] S.J. Turneaure, P. Renganathan, J. Winey, Y. Gupta, Twinning and dislocation evolution during shock compression and release of single crystals: real-time X-ray diffraction, Physical Review Letters. 120 (2018) 265503.

[10] P. Renganathan, J. Winey, Y. Gupta, Shock compression and release of a-axis magnesium single crystals: Anisotropy and time dependent inelastic response, Journal of Applied Physics. 121 (2017) 035901.

[11] A. Gilat, R. Clifton, Pressure-shear waves in 6061-T6 aluminum and alpha-titanium, Journal of the Mechanics and Physics of Solids. 33 (1985) 263–284.

[12] K. Kim, R. Clifton, Pressure-shear impact of 6061-T6 aluminum, (1980).

[13] R. Klopp, R. Clifton, T. Shawki, Pressure-shear impact and the dynamic viscoplastic response of metals, Mechanics of Materials. 4 (1985) 375–385.

[14] S.E. Grunschel, Pressure-shear plate impact experiments on high-purity aluminum at temperatures approaching melt, (2009).

[15] P. Zavattieri, H.D. Espinosa, An examination of the competition between bulk behavior and interfacial behavior of ceramics subjected to dynamic pressure–shear loading, Journal of the Mechanics and Physics of Solids. 51 (2003) 607–635.

[16] J. Millett, S. Stirk, N. Bourne, G. Gray III, On the behaviour of the magnesium alloy, AZ61 to one-dimensional shock loading, Acta Materialia. 58 (2010) 5675–5682.

[17] M. Zhao, V. Kannan, K. Ramesh, The dynamic plasticity and dynamic failure of a magnesium alloy under multiaxial loading, Acta Materialia. 154 (2018) 124–136.

[18] C. Kettenbeil, Dynamic Strength of Silica Glasses at High Pressures and Strain Rates, (2019).

[19] C. Kettenbeil, M. Mello, M. Bischann, G. Ravichandran, Heterodyne transverse velocimetry for pressure-shear plate impact experiments, Journal of Applied Physics. 123 (2018) 125902.

[20] R.J. Clifton, R.W. Klopp, Pressure-shear plate impact testing, Metals Handbook. 8 (1985) 230–239.

[21] C. Kettenbeil, Z. Lovinger, S. Ravindran, Mello, Michael, G. Ravichandran, Pressure-Shear Plate Impact Experiments at High Pressures, (n.d.).

[22] T. Wang, B. Zuanetti, V. Prakash, Shock response of commercial purity polycrystalline magnesium under uniaxial strain at elevated temperatures, Journal of Dynamic Behavior of Materials. 3 (2017) 497–509.

[23] M.A. Meyers, Dynamic behavior of materials, John wiley & sons, 1994.

[24] G. Abaqus, Abaqus 6.11, Dassault Systemes Simulia Corporation, Providence, RI, USA. (2011).

[25] S.P. Marsh, LASL shock Hugoniot data, Univ of California Press, 1980.

[26] J. Johnson, R. Rohde, Dynamic deformation twinning in shock- loaded iron, Journal of Applied Physics. 42 (1971) 4171–4182.

[27] D.-S. Xu, J.-P. Chang, J. Li, R. Yang, D. Li, S. Yip, Dislocation slip or deformation twinning: confining pressure makes a difference, Materials Science and Engineering: A. 387 (2004) 840–844.

[28] https://www.intlmag.org/page/basics_phys_prop_ima, (n.d.).

[29] B. Mishra, A. Mukhopadhyay, K.S. Kumar, D.V. Kumar, K. Jonnalagadda, M. Prasad, Effect of test temperature on flow behavior and strain hardening of magnesium under high strain rate deformation conditions, Materials Science and Engineering: A. 770 (2020) 138546.

[30] R. Plamthottam, S. Lavenstein, J.A. El-Awady, Effect of temperature on the suppression of twinning in textured magnesium, MRS Communications. 9 (2019) 1093–1097.

[31] S. Chen, Y. Li, N. Zhang, J. Huang, H. Hou, S. Ye, T. Zhong, X. Zeng, D. Fan, L. Lu, Capture Deformation Twinning in Mg during Shock Compression with Ultrafast Synchrotron X-Ray Diffraction, Physical Review Letters. 123 (2019) 255501.

[32] A. Arab, Y. Guo, Q. Zhou, P. Chen, A New S-Shape Specimen for Studying the Dynamic Shear Behavior of Metals, Metals. 9 (2019) 838.

[33] S. Ravindran, A. Tessema, A. Kidane, Local deformation and failure mechanisms of polymer bonded energetic materials subjected to high strain rate loading, Journal of Dynamic Behavior of Materials. 2 (2016) 146–156.

[34] S. Ravindran, V. Gupta, A. Tessema, A. Kidane, Effect of Particle Mass Fraction on the Multiscale Dynamic Failure Behavior of Particulate Polymer Composites, Experimental Mechanics. 59 (2019) 599–609.

[35] M.A. Meyers, V.F. Nesterenko, J.C. LaSalvia, Q. Xue, Shear localization in dynamic deformation of materials: microstructural evolution and self-organization, Materials Science and Engineering: A. 317 (2001) 204–225.

[36] J.-Y. Kang, B. Bacroix, R. Brenner, Evolution of microstructure and texture during planar simple shear of magnesium alloy, Scripta Materialia. 66 (2012) 654–657.

[37] O. Anderson, A. Chopelas, R. Boehler, Thermal expansivity versus pressure at constant temperature: A re- examination, Geophysical Research Letters. 17 (1990) 685–688.

Appendix-1

The volumetric thermal expansion as a function of pressure was calculated based on the equation shown below [37],

$$\frac{\alpha}{\alpha_o} = \left(\frac{\rho}{\rho_o}\right)^{\delta} \tag{4}$$

where α and α_o are the volumetric thermal expansion coefficients at densities, ρ and ρ_o, respectively, and δ is the Anderson coefficient. Ratio of the densities can be found in [25]. Using Eq. (4), the variation of the volumetric thermal expansion coefficient as a function of pressure (P) is calculated and is shown in Fig. 6. The fitted function is $\alpha = aExp(mP)$. The coefficients, a and m, are shown in the figure.

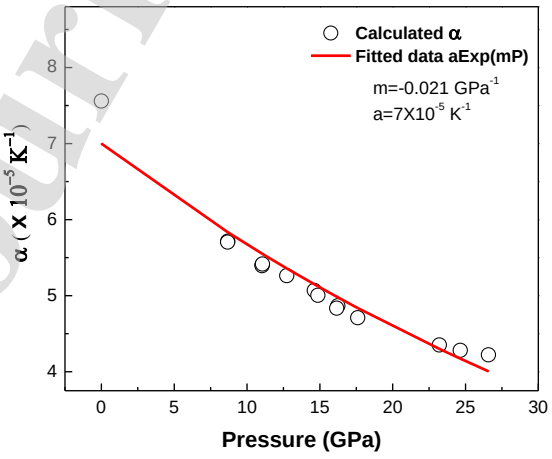

Figure 6. Variation of the volumetric thermal expansion coefficient of expansion as a function of pressure.

Declaration of interests

☒ The authors declare that they have no known competing financial interests or personal relationships that could have appeared to influence the work reported in this paper.

☐The authors declare the following financial interests/personal relationships which may be considered as potential competing interests: